RiESTech
Recent in Engineering Science and Technology

MBI

Article

Analysis of the Effect of Feeder Volume on Shrinkage Porosity Defects in Piston Products through the Gravity Die Casting Process

Nabila Banowati [1], Muhammad Fernanda Alvi Yasin [1], Veronika Noviaty [1], Sugeng Mulyono [1], Tia Rahmiati [1], Wandi Wahyudi [2], Vika Rizkia [1,*]

[1] Mechanical Engineering, Politeknik Negeri Jakarta, Jl. Prof.G.A Siwabessy, Kampus UI, Depok, 16425, Indonesia
[2] Physical Sciences and Engineering (PSE), King Abdullah University of Science and Technology (KAUST), Saudi Arabia 23955
* Correspondence: vika.rizkia@mesin.pnj.ac.id

Abstract: To achieve defect-free casting (soundness casting) with a minimal amount of shrinkage porosity, refinement during the casting process is necessary. In the gravity die casting process, there are parameters that lead to product defects, especially in the casting design, focusing on the gating system and feeder system as pathways for the flow of molten metal to supply the molten metal into the mold cavity. This research was conducted to examine the effect of adding feeder dimensions on shrinkage porosity, specifically on Al-Si piston products with a Silicon content of 12-13%. Feeder dimensions were varied in nine variations by adding height and width to the feeder gate, initially measuring 90mm in height and 32mm in width, along with the addition of insulation to the feeder to retain the heat of the casting process. Cooling used water and argon, with water placed at the center core and pin core and argon placed on the outer mold, with a solidification time of 150 seconds and pouring time of 3 seconds considered constant. This study used a Computer Aided Engineering (CAE) approach, namely MagmaSoft or the application of software to model the gravity casting system process. The results showed the lowest percentage of shrinkage at feeder dimensions of 114mm in height and 45mm in width with a mold temperature of 220°C was 0.76% of the product.

Keywords: Gravity Die Casting; Feeder; Piston; Shrinkage Porosity; Magmasoft Analysis

Citation:. Banowati, N., Yasin, M. F. A., Noviaty, V., Mulyono, S., Rahmiati, T., Wahyudi, W., Rizkia, V. (2024). Analysis of the Effect of Feeder Volume on Shrinkage Porosity Defects in Piston Products through the Gravity Die Casting Process. Recent in Engineering Science and Technology, 2(02), 1–17. Retrieved from https://www.mbi-journals.com/index.php/riestech/article/view/56

Academic Editor: Iwan Susanto

Received: 26 April 2024
Accepted: 29 April 2024
Published: 30 April 2024

Publisher's Note: MBI stays neutral with regard to jurisdictional claims in published maps and institutional affiliations.

1. Introduction

The time-varying temperature profiles significantly impact the occurrence of shrinkage porosity defects in castings during the solidification process. The temperature gradients inside the component dictate whether a location in the process of solidification has adequate access to a higher-temperature feed metal[1,2]. Shrinkage porosity will form in areas where volume decreases as a result of phase shift without any access to the main metal supply. These regions are commonly referred to as "hot spots" due to the presence of islands of hot metal surrounded by colder material[3–5]. The current study focused on a shrinkage porosity problem that one of the automotive companies was trying to fix in their aluminum foundry, as depicted in Figure 1. Shrinkage porosity was present in the crown section, the center of the pin boss, and the pin center of the piston product, which is located near the feed system. According to reports, 90 percent of shrinkage problems occur as a result of inadequate casting design[6–9], which in turn impacts the process of filling the mold and subsequently impacts the mechanical properties of the cast material[10–12].

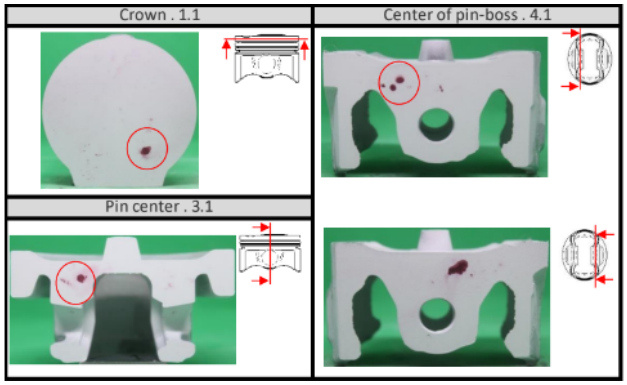

Figure 1. A cross-section of an aluminum alloy piston. The red circles indicate casting walls containing the shrinkage porosity.

The study aimed to discover the effect of feeder dimension and die temperature on shrinkage porosity and determine effective measures to mitigate this defect, ensuring that the parts successfully passed a leak test. Due to the heavy production program, physical experimentation on the manufacturing line was impossible. Therefore, software simulations of the process were suggested instead. In numerous sectors of the industry at present, software simulations are progressively replacing physical experiments[13–16]. Numerical experiments are conducted to determine the optimal process parameters and tooling to ensure that products are manufactured accurately from the first time, thereby avoiding costly and time-consuming physical experimentation. Furthermore, to address casting defects, researchers have developed mathematical models, which were integrated into simulation software[17–21]. MAGMAsoft, renowned for its capabilities in simulating and optimizing casting processes, was utilized for conducting numerical simulations. These numerical simulations were utilized to detect problems virtually. The use of virtual simulations offers several advantages to manufacturers, including improved quality and reduced production costs[22–24].

Gunasegaram et al. utilized numerical simulation and experimental design to establish the key factors that affect the shrinkage porosity in permanent mold castings, aiming to attain an optimal outcome. It was found that the presence of a thick layer of mold, along with a high temperature of the mold, caused a large displacement of shrinkage porosity from critical areas [5]. Dabade et al. utilized the design of experiments and the Taguchi approach to determine the primary process parameter that affects the casting process. To mitigate shrinkage porosity in the cast component, a solidification study was conducted utilizing computer simulation software using innovative gating and feeding methods. Their findings revealed a notable reduction in shrinkage porosity and an enhancement in casting yield [24]. The use of computer simulations to identify casting defects that form during the solidification phase of casting components was investigated by Vijayaram et al. They provided evidence that these simulations benefited the foundry industry significantly[25].

In this study, numerical simulation techniques were utilized to reduce the occurrence of shrinkage porosity defects in the gravity die-casting process. MAGMAsoft was utilized to simulate the cast component in a realistic manner, and the simulation results were integrated into real-time casting. The effect of feeder dimension and die temperature on shrinkage porosity in piston products of one of the automotive companies has become a novelty.

2. Materials and Experiment Methods

This work uses the Magma5 Version 5.3.0 software platform to model the complete casting process. The CAE simulation procedure is executed according to this methodology. CAD software is utilized to create an accurate geometrical model of the gravity die-casting system based on actual dimensions. Pre-processing is the initial stage of analyzing

a computational model. This stage consists of creating boundary conditions and meshing, defining the materials used or determining the domain, defining related parameters, and creating geometry. After that, cavity filling simulation is conducted using the specimen of AC8A (AlSi12CuNiMg) with the pouring and die temperatures of 740°C and 220°C, respectively. In this study, the original design as seen in Table 1. was altered to reduce the occurrence of shrinkage porosity defects in the cast product. This was achieved by modifying the feeder height to 98, 106.5, and 115 mm, and adjusting the feeder gate to 40, 44, and 48 mm. Moreover, post-processing is done after cavity filling simulation in order to simulate the casting process during the solidification stage, including fraction solid solidification, temperature distribution, potential hot spot locations that may result in casting defects, and shrinkage porosity. Once the casting simulation utilizing the CAD technique yields optimal results, the validation is performed by manual gravity die casting as seen in Figure 2. The quality check of validation cast products is done by dye penetrant test and microstructure analysis.

Table 1. Gating system parameters of the initial design

Piston weight (1 cavity)	233.2 gr
Piston volume	84985 mm^3
Feeder height	82 mm
Feeder gate	32 mm

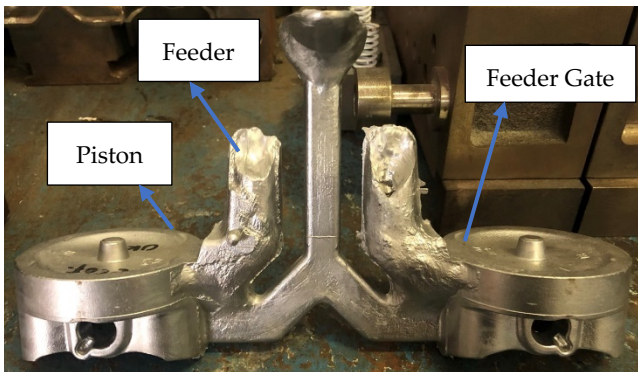

Figure 2. Blank Casting of the Piston

3. Results and Discussion

3.1. Analysis of The Initial Design

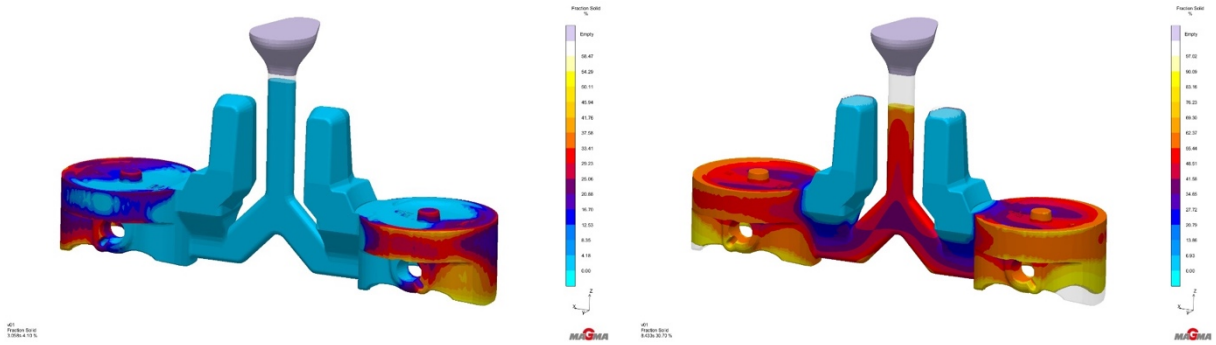

(a) (b)

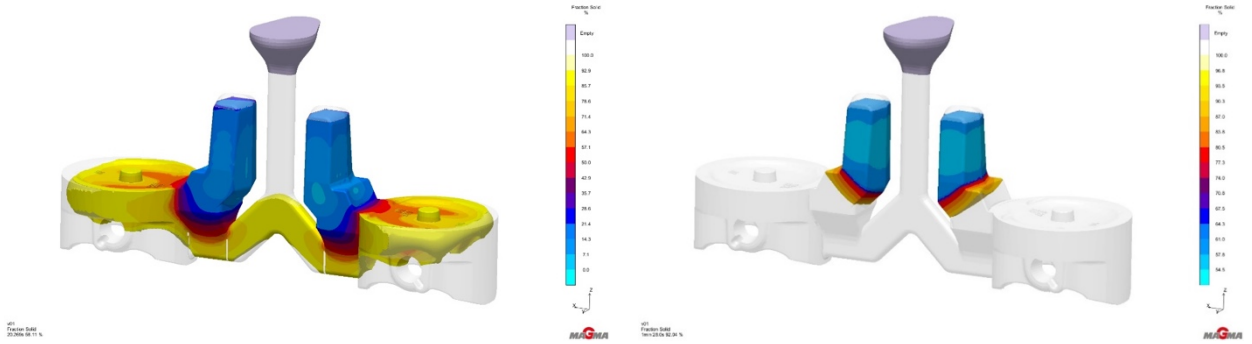

(c) (d)

Figure 3. The phase transition from liquid to solid during solidification at (a) 3.058 s (b) 8.433 s (c) 20.269 s (d) 88s on piston product using initial design

Figure 3. illustrates the phase transition process from liquid to solid. The blue-colored section shows the condition where the molten metal begins to fill the mold cavity, while the sections other than blue indicate the product undergoes solidification. At 3.058 seconds, the product initiates solidification in the outermost region as a result of direct contact with the mold. Solidification continues until approximately 8.433 seconds; at this point, the product turns into a mud phase with 40-70% solid formation, as illustrated in Figure 3(b). At 20.269 seconds (Figure 3(c)), the product solidifies with a solid formation of about 60% to 90%. Moreover, it is noted that the liquid undergoes a transition to become a solid. However, the thickest part adjacent to the feeder gate still exhibits an orange color, indicating that it remains in a liquid metal form. The greater thickness part signifies a deceleration in the solidification process, which may result in shrinkage formation. Upon reaching complete solidification, the final stage of solidification occurs in the gating system, particularly in the feeder section. At 88 seconds, the feeder continues to solidify, allowing it to withdraw any liquid metal from the piston product that has not completely solidified yet, as illustrated in Figure 3(d).

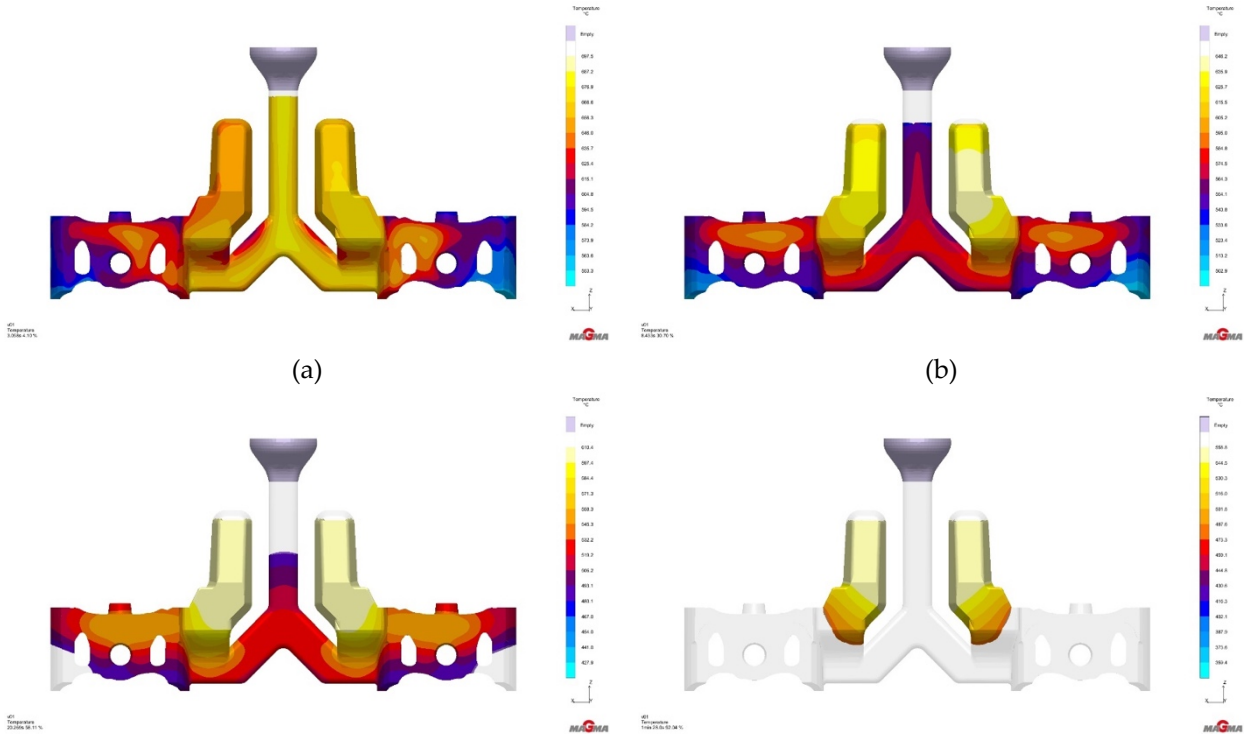

(a) (b)

(c) (d)

Figure 4. Temperature changes during the solidification process at (a) 3.058 s (b) 8.433 s (c) 20.269 s (d) 88s on piston product using initial design

Figure 4. depicts the temperature gradient that occurs during the solidification process. The blue color indicates a temperature decrease as the high-temperature molten metal comes into contact with the mold at 220°C, initiating the transition from liquid to solid. As shown in Figure 4 (a), the molten metal's temperature decreases when it comes into contact with the mold at an initial pouring temperature of 740°C. At 3.058 seconds, the highest temperatures reach 660.7°C and 658.5°C, whereas the temperatures of the solidified cast are 603.9°C and 607.9°C. This temperature difference can cause shrinkage, as depicted in Figures 4(b) and (c). The highest temperatures, reaching 598.7°C and 552.7°C, are found in the thickest part near the pinhole. The part that solidifies faster is the thinnest section of the product. Once this part has solidified, the molten metal cannot fill the voids in the surrounding area. Based on Figure 4, the simulation results have shown uneven temperature distribution during the solidification process, leading to hot spot formation where shrinkage takes place. Therefore, geometric changes are necessary in the feeder system to maximize the supply of molten metal to the product during early solidification stages.

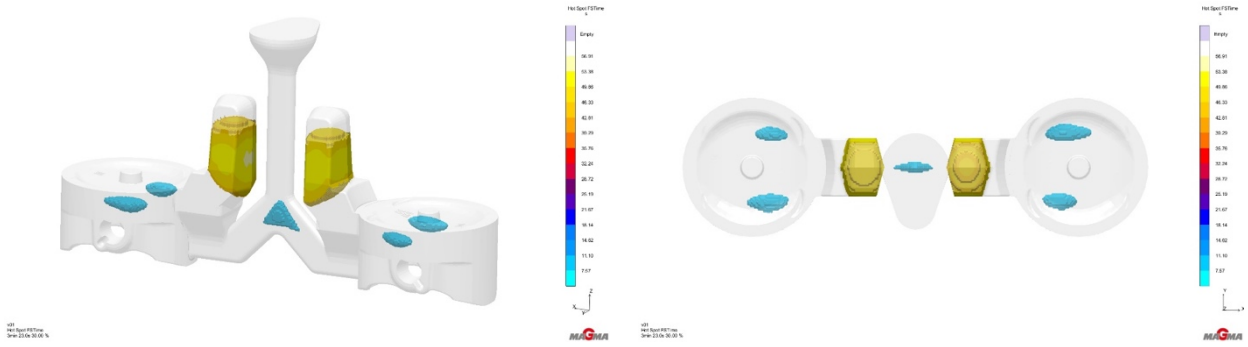

(a) (b)

Figure 5. The critical points where defects are likely to occur

Hot spots indicate the solidification time at the peak area from the liquidus to the temperature where there is no longer a supply flow from the feeder system. As a result, they represent the highest temperature implemented from the effectiveness value of the supply stored in the alloy material dataset, depicting the solidified molten parts and the potential for defects. Figure 5(a) and (b) display the front view and the top view, respectively, of the critical points (hot spots) corresponding to the hottest temperature when the product reaches 100% solid condition.

There is a potential for shrinkage porosity defects evident from the location of critical points (Hot Spots) on the crown, center of pin-boss, and pin center near the feeder system, as shown in Figure 1. The image confirms that the porosities formed during the final stages of solidification with the product at 100% solid condition align with their critical point locations due to temperature discrepancies during the solidification process. These areas experience slower solidification compared to thinner sections, resulting in insufficient material supply from the feeder system. The shrinkage porosity magnitude formed from 2 cavities amounts to 11.33%. Generally, it is advantageous that approximately 90% of the shrinkage occurs in the feeder rather than in the product. To address this issue, adjustments in feeder height, feeder gate width, and the addition of insulation to the feeder system are necessary to retain heat from the casting process and prevent gas bubble formation due to the molten metal's heat. Additionally, monitoring mold temperatures is crucial to guide solidification effectively.

3.2. Analysis of Modification Design

In order to address shrinkage porosity defects, modifications are made to the feeder dimensions as seen in Table 2. In this study, adjustments will be made to increase the height and width of the feeder gate, as well as the addition of insulation to retain heat during the casting process.

Table 2. Design variation in feeder system dimension

Design	Feeder height (mm)	Feedergate width (mm)
1	98	40
2	98	44
3	98	48
4	106.5	40
5	106.5	44
6	106.5	48
7	115	40
8	115	44
9	115	48

The solidification rate significantly influences the strength and hardness of the product. The casting process for this type of piston typically requires a solidification time of around 150 seconds based on field trials with favorable outcomes. Total solidification time refers to the duration of the molten metal being poured until the mold is opened again in the gravity casting process. In this research, the Magma software provides information about the optimal solidification flow of the product in percentage at specific temperatures. Figure 6. depicts comparisons of the transition from liquid to solid for each variation.

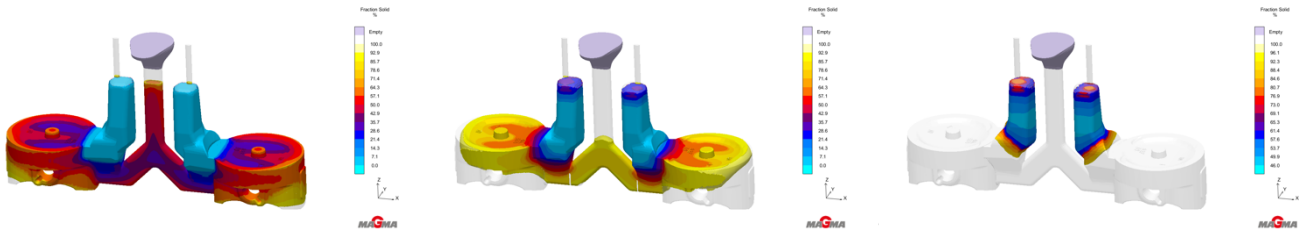

(a)

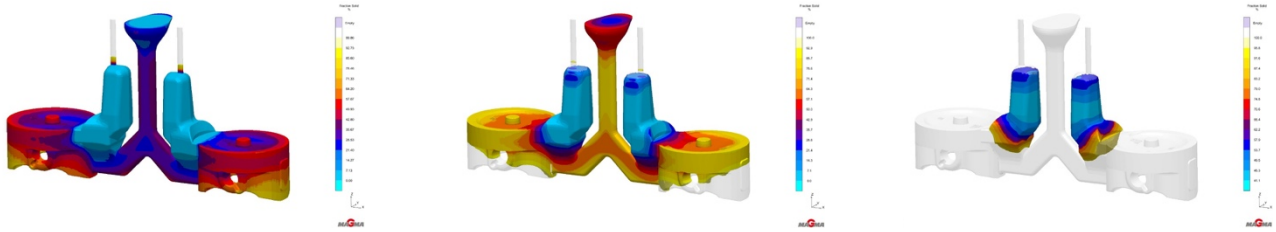

(b)

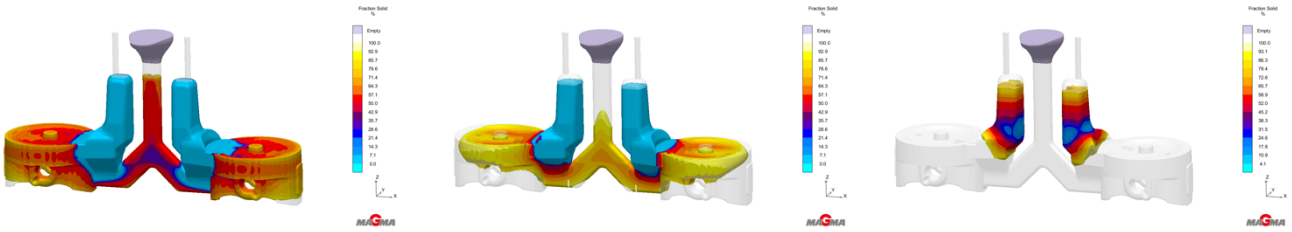

(c)

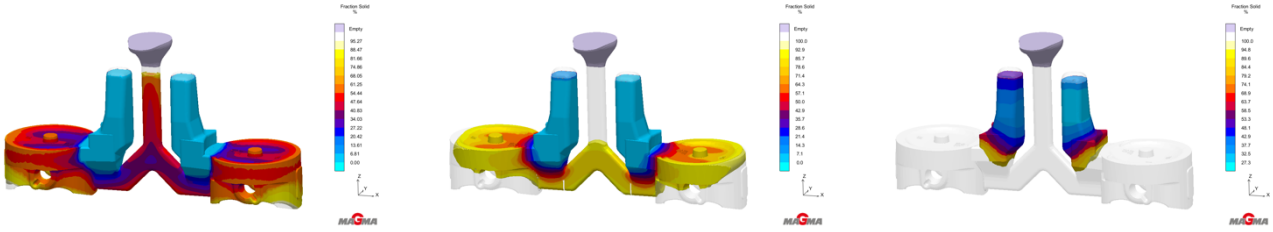

(d)

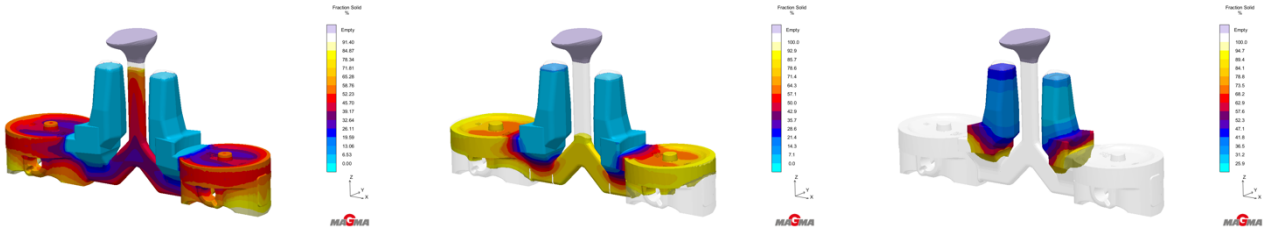

(e)

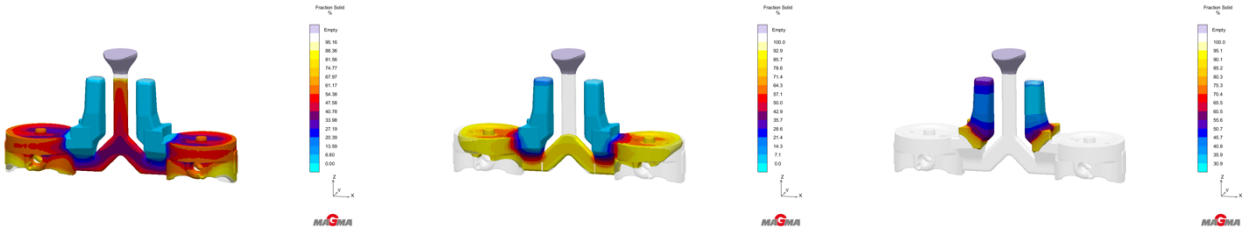

(f)

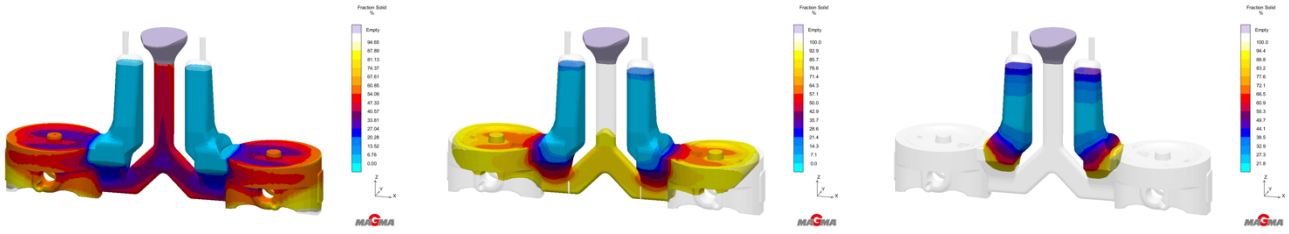

(g)

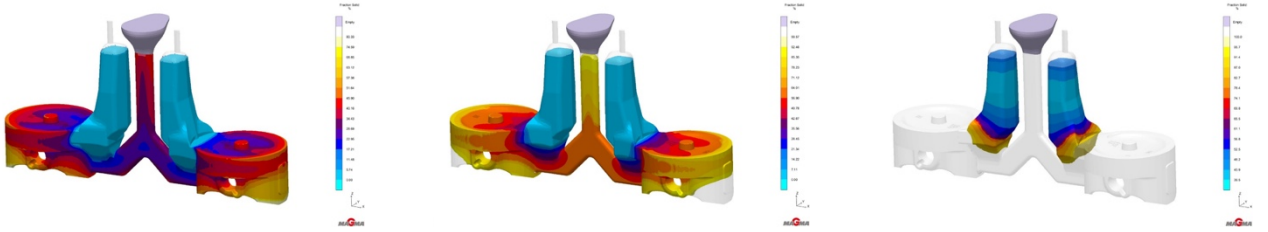

(h)

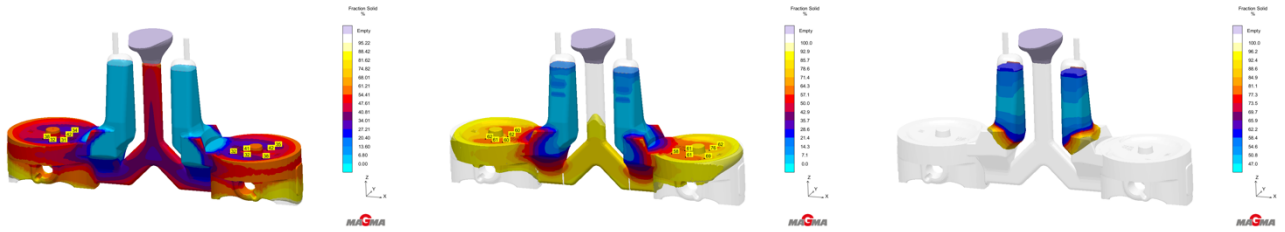

(i)

Figure 6. Solid fraction of all designs (a) 1st variation, (b) 2nd variation (c) 3rd variation (d) 4th variation (e) 5th variation, (f) 6th variation, (g) 7th variation, (h) 8th variation, (i) 9th variation, observed at time intervals of 8.433 s, 20.269 s, and 88 s from left to right.

As depicted in Figure 6, the solidification process simulation is represented in percentage (%) at specific periods. The uniformity of the solidification process is denoted by the colors of blue, yellow, red, and orange. Blue indicates that the product is still in the liquid phase; yellow implies complete solidification; and red and orange signify the product is in the mud phase, meaning that the phase transition from liquid to solid is not yet complete. Although no substantial changes are observed among the nine variations, the final solidification can be seen forming in the feeder system. Moreover, the eighth variation demonstrates a more uniform solidification in comparison to the others. Moreover, during the solidification process at 20.269 seconds, the thickest section near the feeder gate retains an orange color, indicating that it remains in a liquid metal state. However, there is still enough supply of material from the feeding system, indicated by a large red color, to fill the vacancies within the mold cavity.

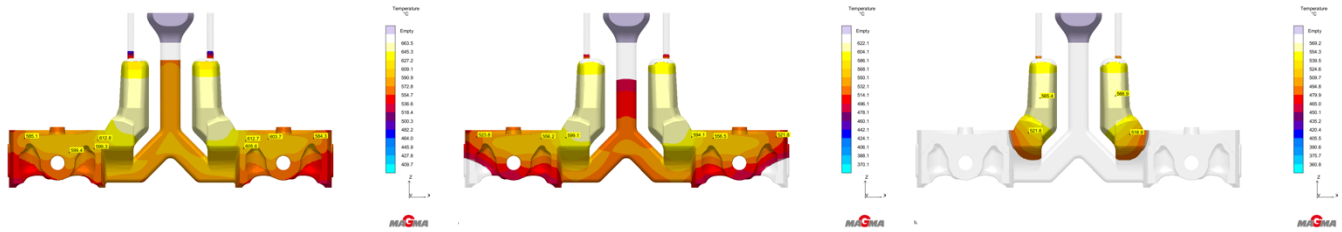

(a)

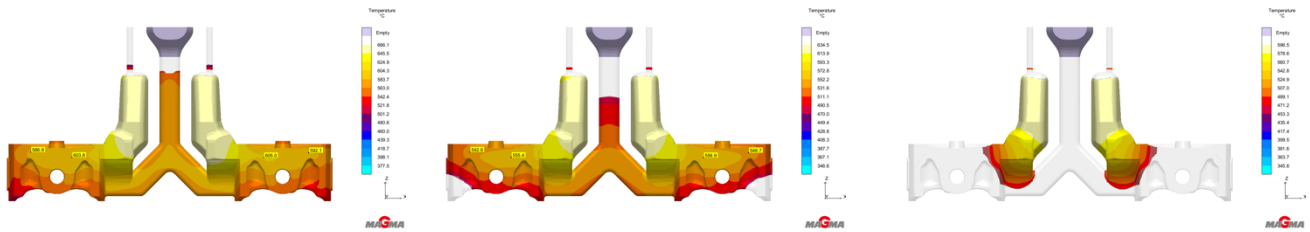

(b)

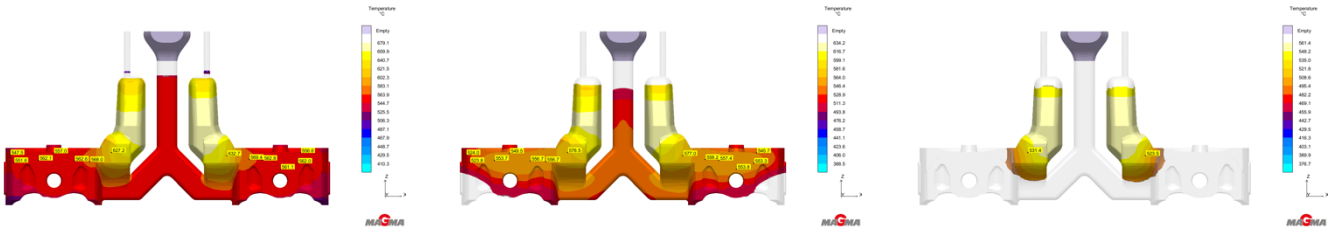

(c)

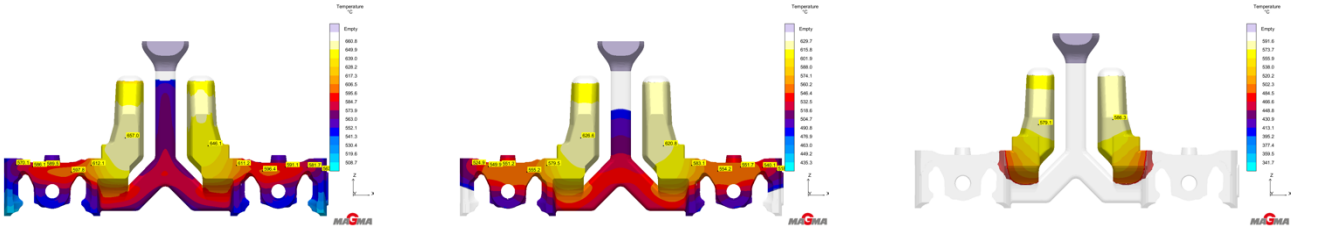

(d)

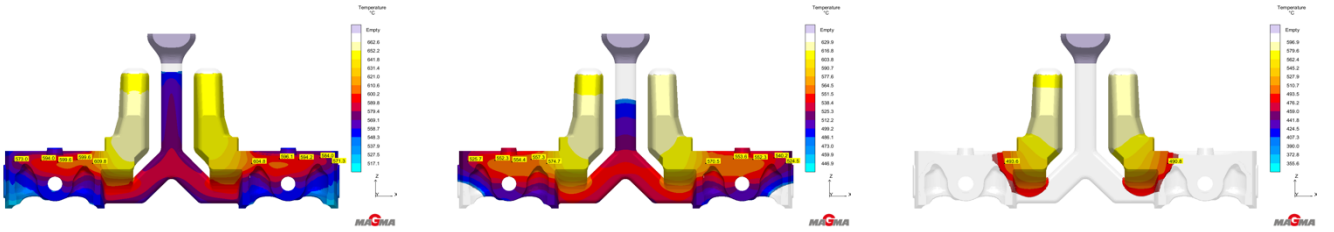

(e)

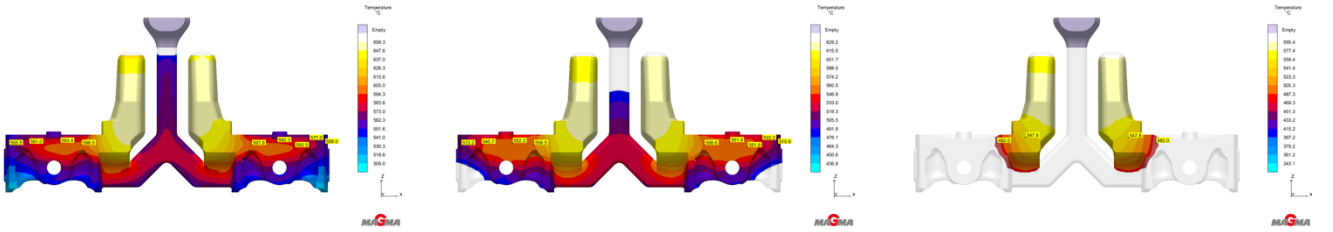

(f)

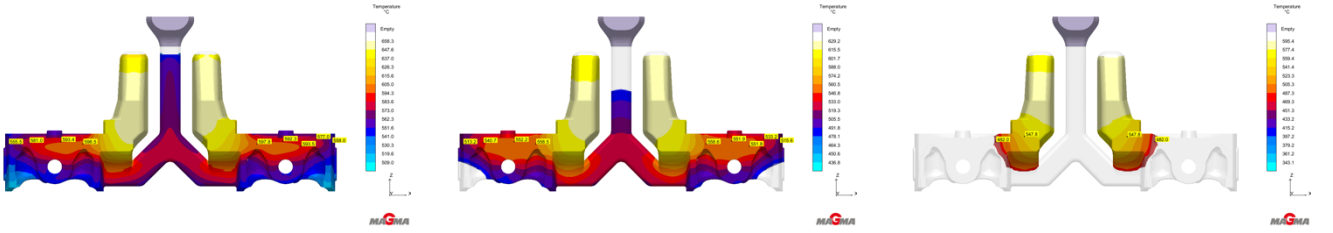

(g)

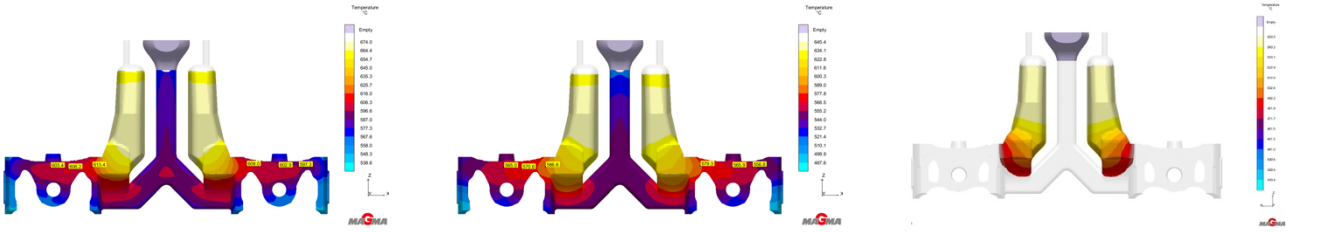

(h)

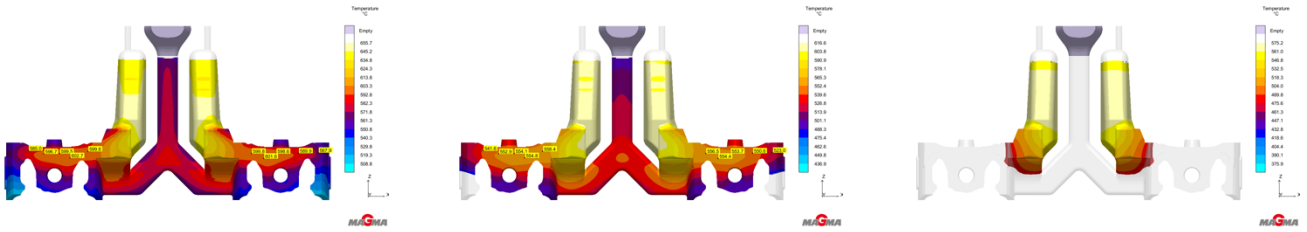

(i)

Figure 7. Distribution temperature of all designs (a) 1st variation, (b) 2nd variation (c) 3rd variation (d) 4th variation (e) 5th variation, (f) 6th variation, (g) 7th variation, (h) 8th variation, (i) 9th variation, observed at time intervals of 8.433 s, 20.269 s, and 88 s from left to right.

Figure 7 illustrates the distribution temperature (gradient temperature) during the solidification process. The image displays color variations indicating temperature changes from the initial pouring until the moment when the metal fills the whole mold. Analysis was conducted by observing temperature changes in regions susceptible to shrinkage porosity, namely the side core of the anti-feed gate, feed gate, and feeder sections at solidification times of 8.433 s, 20.269 s, and 88 s. Among the nine (9) variations examined, variation 8 demonstrates the most uniform temperature change at 88 seconds, indicating nearly complete solidification in the potentially defective areas. As depicted in Figure 7, these vulnerable areas have temperatures equivalent to the furthest section of the feeder system, specifically the side core of the anti-feed gate, which is approximately 500°C. Temperatures at the side core anti-feed gate consistently remain lower compared to the feed gate and feeder sections due to their contact with the mold. This phenomenon is associated with the higher thermal conductivity of the mold, facilitating quicker solidification when the molten metal, at high temperatures, comes into contact with the mold. Temperatures at the feed gate and feeder sections appear higher, approximately around 600°C. This indicates that the phase in these sections has not fully transitioned into solid form, thus still capable of filling voids in the mold cavity and consequently reducing the potential for shrinkage porosity.

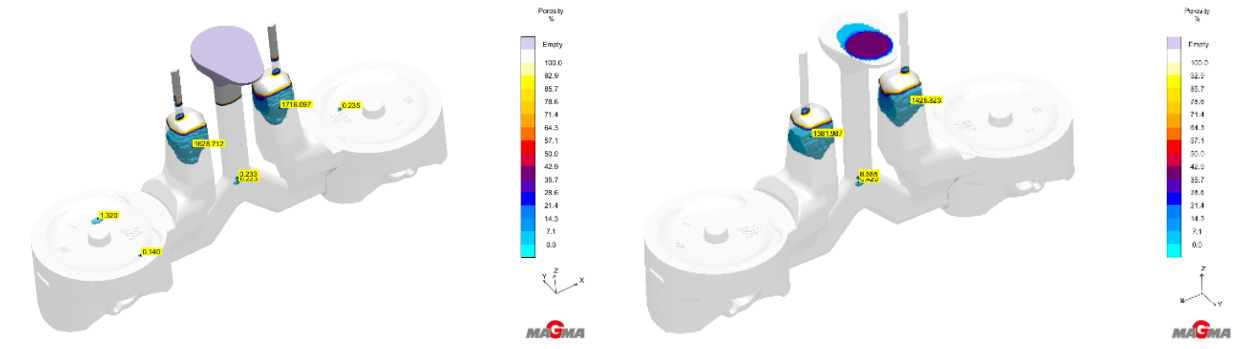

(a) (b)

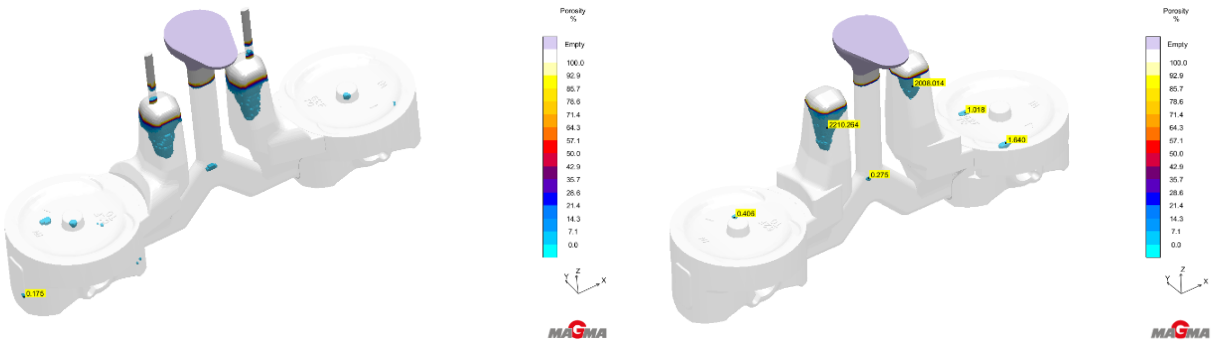

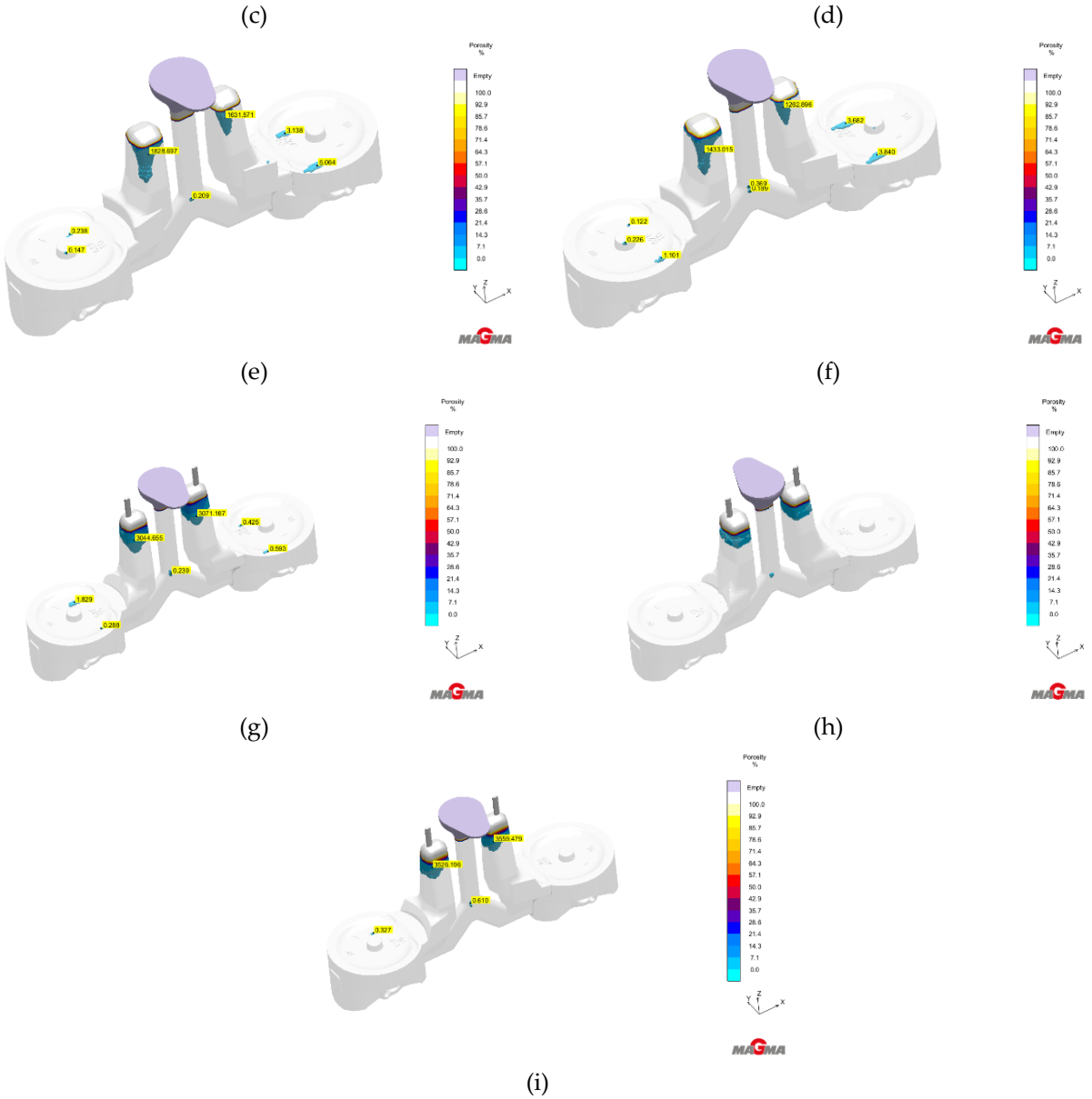

Figure 8. The position of shrinkage porosity of (a) 1st, (b) 2nd, (c) 3rd, (d) 4th, (e) 5th, (f) 6th, (g) 7th, (h) 8th, (i) 9th

Figure 8. illustrates the location and percentage of shrinkage for each variation tested. Shrinkage is more prevalent in the thickest sections than in other areas due to inadequate supply from the feeder system. As seen in Figure 8, integrating a feeder into the gating system facilitates the intake of additional material during the solidification process, effectively filling the reduced volume of molten metal in the mold. Consequently, the feeder serves as the final freezing point within the system. As a result, any shrinkage porosity that occurs will manifest in the feeder instead of the piston product. Among the nine (9) variations examined, variation 8 demonstrates that hot spots do not occur on the product, but are only found within the feeder system and its runner components. The porosity percentage values obtained from the analysis using Magmasoft 5.3 are presented in Table 3.

Table 3. The percentage and volume of shrinkage porosity for all tested variations

Var	Shrinkage prosity percentage (%)			Total Porosity (%)	Shrinkage porosity volume (mm^3)			Total shrinkage volume (mm^3)
	Runner	1st Cav	2nd Cav		Runner	1st Cav	2nd Cav	
1st	0.456	1.46	0.235	2.15	87.73	1240.78	199.71	1528.23
2nd	1.094	0	0	1.09	210.49	0.00	0.00	210.49
3rd	0.12	2.19	2.19	4.5	23.09	1861.17	1861.17	3745.43
4th	0.275	0.406	2.658	3.34	52.91	345.04	2258.90	2656.85
5th	0.209	0.385	8.202	8.79	40.21	327.19	6970.47	7337.87
6th	0.558	1.454	7.542	9.53	107.36	1235.68	6409.57	7752.61
7th	0.239	2.117	1.018	3.37	45.98	1799.13	865.15	2710.26
8th	0.758	0	0	0.76	145.84	0.00	0.00	145.84
9th	0.729	0.327	0	1.056	140.26	277.90	0.00	418.16

Table 3 illustrates the percentage and volume of Shrinkage Porosity in 9 variations of feeder size designs feeder size designs following simulation utilizing software feeder size designs following simulation utilizing Magmasoft. According to the table, the lowest porosity percentage is shown by the 8th variation, with a feeder height of 115 mm and feeder gate (ingate) of 45 mm, resulting in a shrinkage of 0.76% of the total casting product volume. The calculated volume of shrinkage porosity formed in the 8th variation is 145.84 mm^3 out of a total volume of 84985 mm^3. Furthermore, shrinkage porosity occurs in the runner rather than the product, where this part will not be used. The analytical results indicate that the width of the feeder gate has a significant impact on the occurrence of shrinkage. If the feeder width is too narrow, there will be an inadequate supply of molten metal to fill the empty spaces in the mold cavity during compaction. Nevertheless, if the size of the feeder gate is excessively large, it might induce an overabundance of material flow and a rapid flow rate, which can contribute to turbulence and subsequently cause shrinkage at multiple locations.

3.3. Dye Penetrant and Microstructural Analysis

To check the quality of cast products after simulation, the cast pistons were nondestructively tested using the dye penetrant method and microstructure analysis.

Initial Design

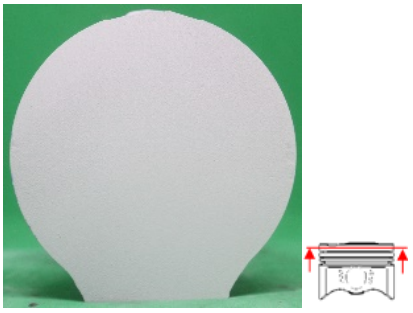

(a)

The 8th Variation

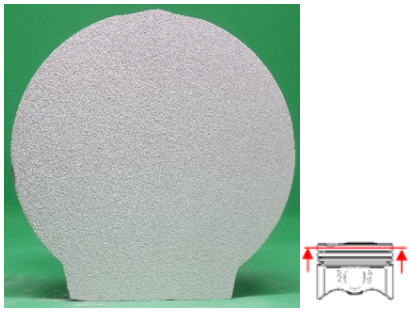

(b)

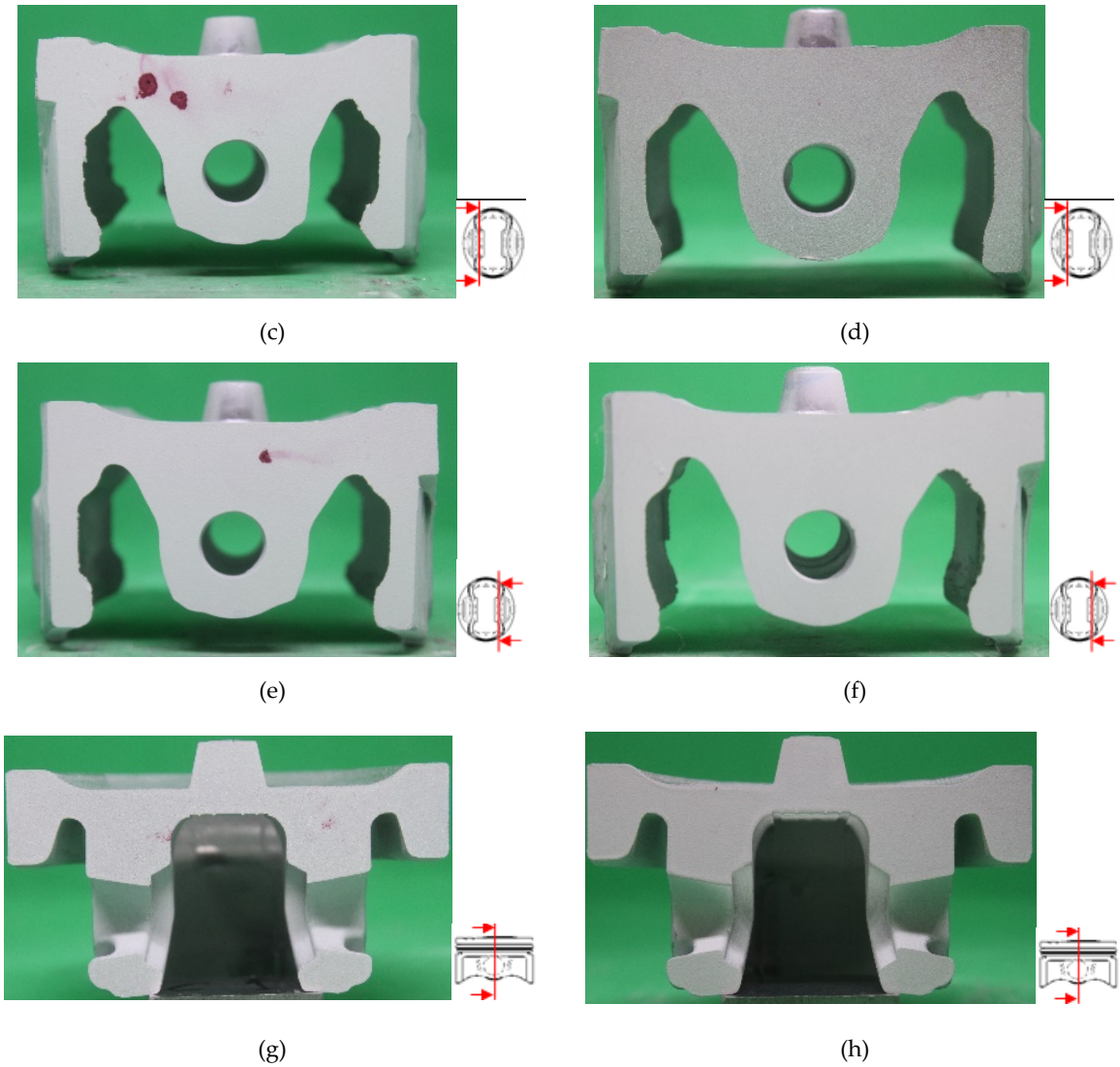

Figure 9. Comparison of dye penetrant test on (a) crown of initial design, (b) crown of 8th variation, (c) left side of pin-boss of initial design, (d) left side of pin-boss of 8th variation (e) right side of pin-boss of initial design (f) right side of pin-boss of 8th variation (g) pin center of initial design (h) pin center of 8th variation design

Figure 9. illustrates a comparison of the dye penetrant test results on the product before and after the modification of the gating system (8th variation). Among the nine variations tested in this study, variation eight emerged as the optimal configuration, featuring a feeder height of 115 mm and a feeder gate width of 44 mm. This particular variation resulted in a porosity percentage of 0.76% as determined by Computer-Aided Engineering (CAE) analysis. As can be seen in Figure 9, complete casting using the initial design exhibits porosity in the pin boss and pin center, as indicated by the red color observed by penetrant testing. This was due to the initial design producing the cooling process that led to the failure of timely feeding of molten metal. Moreover, the high thickness of the piston product is also a contributing factor to the occurrence of more shrinkage porosity. However, dye penetrant observation of the piston cast obtained from the 8th variation shows no porosities emerging within the product. This phenomenon is in good

agreement with the Magma simulation results, which indicated that the shrinkage porosity was only about 0.76% and primarily located in the feeder system and its runner components. As a result, the simulation accuracy in Figure 8 (h) is highly confirmed.

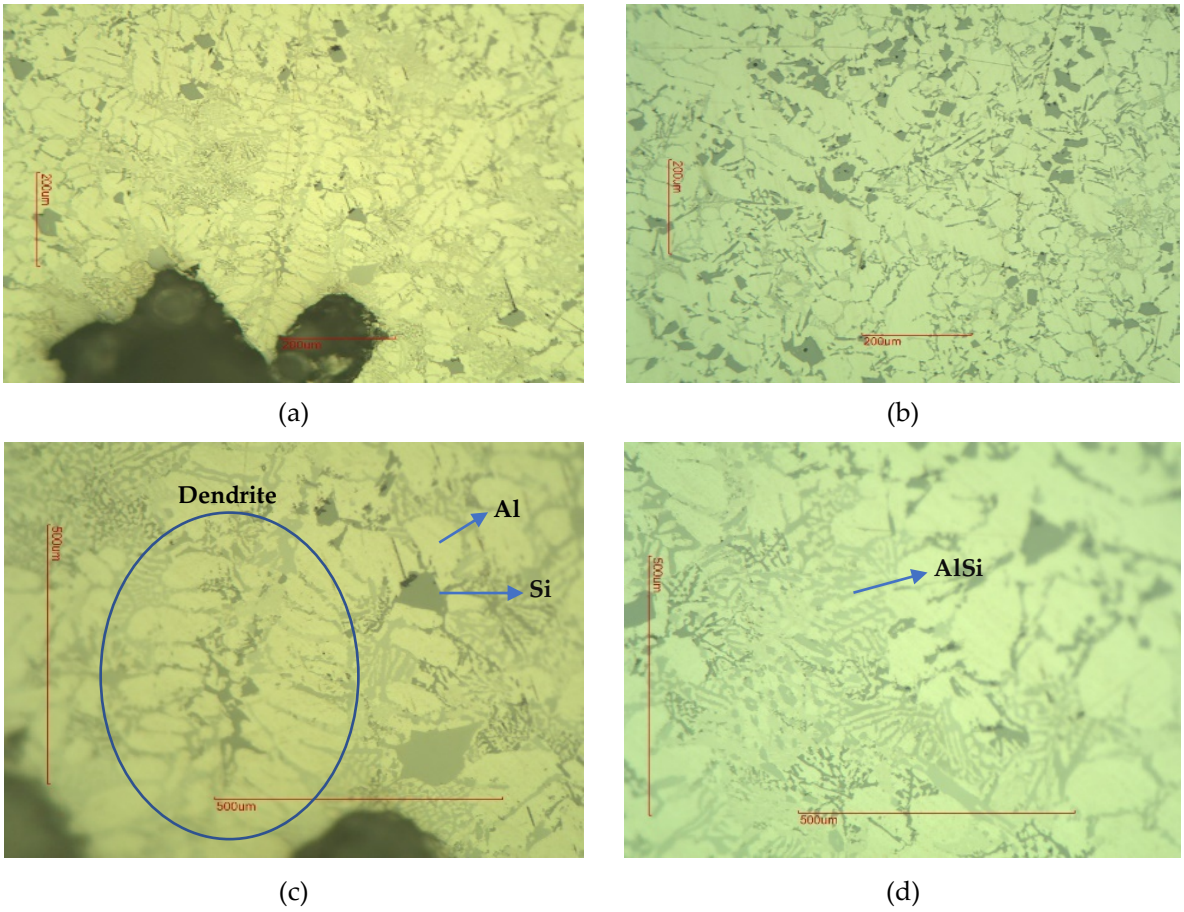

Figure 10. The optical micrographs depict the microstructures of the pin boss of the casting piston acquired from the original design of the gating system

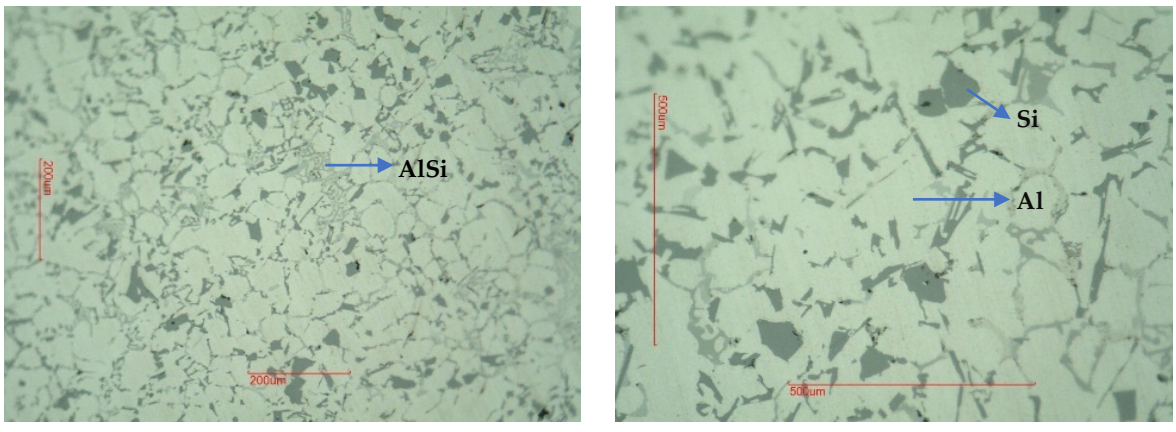

Figure 11. The optical micrographs depict the microstructures of the pin boss of the casting piston acquired from the 8th variation design of the gating system

Figure 10. displays the microstructure, revealing the shrinkage porosity of a cast piston utilizing a feeder system with dimensions of 90 mm in height and 32 mm in width. The microstructure exhibits a shrinkage porosity defect covering an area of 15,945.278 mm^2, which accounts for 17.378% of the total examined area. The impractical system of the cooling process in the initial design result in the failure to provide molten AC8A alloy adequately. The significant difference in thickness within the pin center and pin boss parts contributes to an increased occurrence of shrinkage porosity. This essentially confirms the accuracy of the simulation results. Moreover, Figure 11. reveals the microstructure of a piston product in the absence of shrinkage porosity. In general, the microstructure of both unmodified and modified gating systems consists of primary α-Al phase, primary Si, and eutectic Al-Si[26]. In addition, the major α-Al phase displayed two distinct forms: larger Al grains that developed in the shrinkage porosity due to slower cooling rates, and smaller Al grains that formed in the remaining sections with faster cooling rates. The larger Al grains exhibited dendritic or rosette-like morphology, as illustrated in Figure 10(c), whereas the smaller Al phase exhibited more equiaxial grains, as depicted in Figure 11(b).

4. Conclusions

In this study, a set of AlSi12CuNiMg gravity die-casting experiments has been conducted to solve the problem of shrinkage porosity in the cast piston industry. The analysis using a Computer-Aided Engineering (CAE) approach with the MagmaSoft numerical simulation on the effects of feeder height and feeder gate on the piston product led to the following conclusions:

1. An inadequate dimension of feeder height and feeder gate will result in an insufficient flow volume supply to the product. According to the simulation results, the maximum shrinkage porosity defect of 9.53% was generated at a feeder height of 106 mm and a feeder gate width of 48 mm. The microstructure analysis confirmed the existence of dendrites in the vicinity of the shrinkage porosity.
2. The most optimal variation was found to be a feeder height of 115 mm and a feeder gate width of 45 mm, which resulted in a shrinkage porosity of 0.76% in gating system.

References

1. B. Bhedasgaonkar, Casting Defect Analysis using Design of Experiments (DoE) and Computer Aided Casting Simulation Technique, Procediassure aluminum alloy casting, Journal of Materials Research and Technology 28 (2024) 4488–4497. https://doi.org/https://doi.org/10.1016/j.jmrt.2023.12.270.
2. B. Dybowski, A. Kiełbus, Ł. Poloczek, Effects of die-casting defects on the blister formation in high-pressure die-casting aluminum structural components, Eng Fail Anal 150 (2023) 107223. https://doi.org/https://doi.org/10.1016/j.engfailanal.2023.107223.
3. R. Wang, Y. Zuo, Q. Zhu, X. Liu, J. Wang, Effect of temperature field on the porosity and mechanical properties of 2024 aluminum alloy prepared by direct chill casting with melt shearing, J Mater Process Technol 307 (2022) 117687. https://doi.org/https://doi.org/10.1016/j.jmatprotec.2022.117687.
4. S. Bhagavath, Z. Gong, T. Wigger, S. Shah, B. Ghaffari, M. Li, S. Marathe, S. Karagadde, P.D. Lee, Mechanisms of gas and shrinkage porosity formation in solidifying shear bands, J Mater Process Technol 299 (2022) 117338. https://doi.org/https://doi.org/10.1016/j.jmatprotec.2021.117338.
5. D.R. Gunasegaram, D.J. Farnsworth, T.T. Nguyen, Identification of critical factors affecting shrinkage porosity in permanent mold casting using numerical simulations based on design of experiments, J Mater Process Technol 209 (2009) 1209–1219. https://doi.org/https://doi.org/10.1016/j.jmatprotec.2008.03.044.

6. S.L. Nimbulkar, R.S. Dalu, Design optimization of gating and feeding system through simulation technique for sand casting of wear plate, Perspect Sci (Neth) 8 (2016) 39–42. https://doi.org/https://doi.org/10.1016/j.pisc.2016.03.001.
7. H. Bhatt, R. Barot, K. Bhatt, H. Beravala, J. Shah, Design Optimization of Feeding System and Solidification Simulation for Cast Iron, Procedia Technology 14 (2014) 357–364. https://doi.org/10.1016/j.protcy.2014.08.046.
8. H. Iqbal, A.K. Sheikh, A. Al-Yousef, M. Younas, Mold Design Optimization for Sand Casting of Complex Geometries Using Advance Simulation Tools, Materials and Manufacturing Processes 27 (2012) 775–785. https://doi.org/10.1080/10426914.2011.648250.
9. T. Wang, S. Yao, Q. Tong, L. Sui, Improved filling condition to reduce casting inclusions using the submerged gate method, J Manuf Process 27 (2017) 108–113. https://doi.org/https://doi.org/10.1016/j.jmapro.2017.01.013.
10. D.G. Eskin, Suyitno, L. Katgerman, Mechanical properties in the semi-solid state and hot tearing of aluminium alloys, Prog Mater Sci 49 (2004) 629–711. https://doi.org/https://doi.org/10.1016/S0079-6425(03)00037-9.
11. D.M. Stefanescu, Computer simulation of shrinkage related defects in metal castings – a review, International Journal of Cast Metals Research 18 (2005) 129–143. https://doi.org/10.1179/136404605225023018.
12. E. 'Giller, N. 'Rensing, P. 'Zavracky, Method for producing high quality optical parts by casting, US20060192307A1, 2006.
13. R. Kumar, S. Madhu, K. Aravindh, V. Jayakumar, G. Bharathiraja, A. Muniappan, Casting design and simulation of gating system in rotary adaptor using procast software for defect minimization, Mater Today Proc 22 (2020) 799–805. https://doi.org/https://doi.org/10.1016/j.matpr.2019.10.156.
14. C. Lei, Y. Yang, G. Yang, Y. Huang, Magma software simulation assisted optimization of the casting system of turbocharger castings, Procedia Manuf 37 (2019) 59–65. https://doi.org/https://doi.org/10.1016/j.promfg.2019.12.013.
15. C.M. Choudhari, B.E. Narkhede, S.K. Mahajan, Casting Design and Simulation of Cover Plate Using AutoCAST-X Software for Defect Minimization with Experimental Validation, Procedia Materials Science 6 (2014) 786–797. https://doi.org/https://doi.org/10.1016/j.mspro.2014.07.095.
16. K. Chen, X. He, Z. Liu, G. Li, P. Zhang, H. Liu, Porosity forming mechanism and numerical simulation of casting process optimization of nickel-based heat-resistant alloy electrode ingot with large height to diameter ratio, Journal of Materials Research and Technology 29 (2024) 2363–2375. https://doi.org/https://doi.org/10.1016/j.jmrt.2024.01.211.
17. G. Timelli, G. Camicia, S. Ferraro, R. Molina, Effects of grain refinement on the microstructure, mechanical properties and reliability of AlSi7Cu3Mg gravity die cast cylinder heads, Metals and Materials International 20 (2014) 677–686. https://doi.org/10.1007/s12540-014-4013-2.
18. H. Yang, S. Ji, D. Watson, Z. Fan, Repeatability of tensile properties in high pressure die-castings of an Al-Mg-Si-Mn alloy, Metals and Materials International 21 (2015) 936–943. https://doi.org/10.1007/s12540-015-5108-0.
19. M. Vlach, J. Čížek, V. Kodetová, T. Kekule, F. Lukáč, M. Cieslar, H. Kudrnová, L. Bajtošová, M. Leibner, P. Harcuba, J. Málek, V. Neubert, Annealing Effects in Cast Commercial Aluminium Al–Mg–Zn–Cu(–Sc–Zr) Alloys, Metals and Materials International 27 (2021) 995–1004. https://doi.org/10.1007/s12540-019-00499-6.
20. K. Min, K. Kim, S.K. Kim, D.-J. Lee, Effects of oxide layers on surface defects during hot rolling processes, Metals and Materials International 18 (2012) 341–348. https://doi.org/10.1007/s12540-012-2020-8.
21. R. Haghayeghi, E. Ezzatneshan, H. Bahai, L. Nastac, Numerical and experimental investigation of the grain refinement of liquid metals through cavitation processing, Metals and Materials International 19 (2013) 959–967. https://doi.org/10.1007/s12540-013-5008-0.
22. S. Yue, G. Wang, F. Yin, Y. Wang, J. Yang, Application of an integrated CAD/CAE/CAM system for die casting dies, J Mater Process Technol 139 (2003) 465–468. https://doi.org/https://doi.org/10.1016/S0924-0136(03)00506-5.

23. L. Patnaik, I. Saravanan, S. Kumar, Die casting parameters and simulations for crankcase of automobile using MAGMAsoft, Mater Today Proc 22 (2020) 563–571. https://doi.org/https://doi.org/10.1016/j.matpr.2019.08.208.
24. U.A. Dabade, R.C. Bhedasgaonkar, Casting Defect Analysis using Design of Experiments (DoE) and Computer Aided Casting Simulation Technique, Procedia CIRP 7 (2013) 616–621. https://doi.org/https://doi.org/10.1016/j.procir.2013.06.042.